8th U. S. National Combustion Meeting
Organized by the Western States Section of the Combustion Institute
and hosted by the University of Utah
May 19-22, 2013

Angle-Dependent Light Scattering Measurements of Silica Aggregates in a Stoichiometric Methane/Hexamethydisiloxane/Air Premixed Flames

J. D. Herdman[1], *H. B. Levinsky*[1,2], *A. V. Mokhov*[1]

[1]*Laboratory for High Temperature Energy Conversion Processes, Energy and Sustainability Research Institute, University of Groningen, Nijenborgh 4, 9747 AG Groningen, The Netherlands*
[2]*DNV KEMA Energy & Sustainability, Nederland B. V. – P.O. Box 2029, 9704 CA Groningen, The Netherlands*

Angle-dependent light scattering (ADLS) measurements have been used in the past to study various fractal structures produced in flames such as soot, titania, and silica. These measurements provide an unobtrusive way to measure the size of fractal aggregates via the calculation of the fractal dimension (D_f) and radius of gyration (R_g) without the use of transmission electron microscopy (TEM). In this study, angle-dependent light scattering was performed on a stoichiometric one-dimensional methane/hexamethyldisiloxane/air premixed flames. Fractal aggregate growth was studied as a function of flame height at various silicon concentrations. The average radius of gyration for aggregates at a specific height above the burner was determined using the Guinier analysis method.

1. Introduction

The International Energy Agency (IEA) is a group of twenty-eight countries, including both the Netherlands and the United States, that are dedicated to both energy security and the research of clean energies, specifically those that help reduce negative effects on the environment. According to the 2012 Oil and Gas Security report on the Netherlands, oil and natural gas are the main sources of the country's total primary energy supply (TPES), making up 85% (38% and 47% respectively) of the TPES in 2010. The rest of the TPES for 2010 consisted of coal (9.5%), renewable energy sources (4.5%), and nuclear energy (1%). In the past twenty years the use of coal has dropped by over five percent due largely to the implementation of renewable energy, specifically biomass energy sources. The use of renewable energy sources are to increase by 2020. In 2010 only 4% of energy consumed was from renewable sources. However, the European Directive on Renewable Energy has appropriated this number to be 14% by 2020 (International Energy Agency, Ministry of Economic Affairs). The Dutch government is rising to this challenge and has outlined initiatives to make this a reality in their 2011 Energy Report (Ministry of Economic Affairs).

In the United States, the TPES for 2011 breaks down as follows: oil and natural gas were 36% and 26% respectively, coal provided 20% of the primary energy, nuclear energy was at 8%, and renewable energy sources consisted of 9% of the primary energy supply (Office of Survey Development and Statistical Integration). Currently there are no mandated national standards or future goals for the US renewable energy consumption. This looks to change in the near future according to President Obama's most recent State of the Union Address (Corasaniti). Until then, however, at least thirty states and the District of Columbia have renewable portfolio standards (RPS). RPS require or encourage electricity in the respective state to be produced through renewable energy means. Some of these states have even laid out quantitative goals for the future (US Energy Information Agency). A side by side breakdown of the TPSE for both the Netherlands and the United States can be seen in Figure 1.

One of the major sources of renewable energy are biofuels consisting of biomass. Biomass are organic materials such as wood, sewage, agricultural waste, food waste, and waste from landfills (Pronobis, Virmond, W. Wang). These have become more attractive in recent years because of their environmental friendliness. Biomass use carbon dioxide during photosynthesis (either during their lifetime such as plants or are associated with plants, e.g. consume plants) and therefore their net carbon emissions after combustion are considered to be neutral (Virmond, Vassilev, Saidur). These sources are not purely organic, however, and tend to have trace amounts of other elements such as potassium, sodium, calcium, magnesium, chlorine, and silicon (Pronobis, Vamvuka). The composition of biomass vary greatly depending on the product, the geographical location in which the product was produced, various agricultural practices that may be in place in a given region, and processing procedures of such waste. Some techniques such as leaching (or washing) have been studied in order to help eliminate the harmful impurities found in biomass, but even that is not 100% effective (Vamvuka).

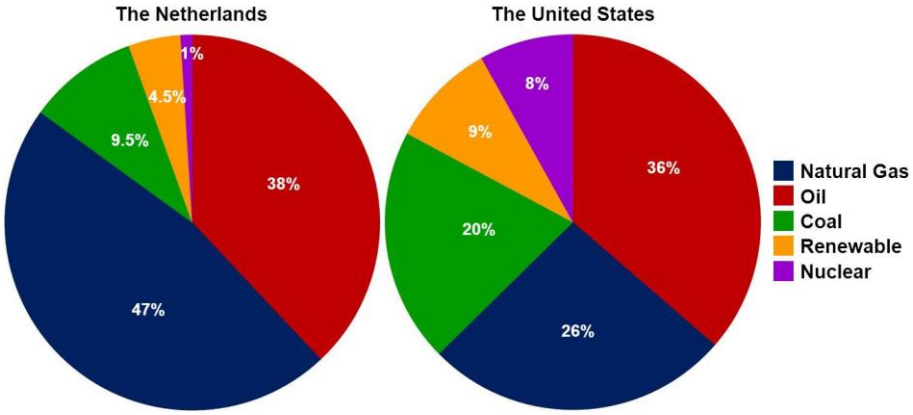

Figure 1. Breakdown of the total primary energy supply for the Netherlands in 2010 (International Energy Agency) and the United States in 2011 (Office of Survey Development and Statistical Integration).

Most appliances, furnaces, boilers, and automobiles that are a target for the use of biofuels currently run on fossil fuels such as natural gas, oil, and coal. These fossil fuels do not possess the impurities that can be present in biomass. This causes a problem when trying to employ biofuels or a mixture of fossil fuels and biofuels. As these impurities combust, different compositions of ash are created some of which may contain large aggregates. These large aggregates may cause damage or inefficiency (e.g. slagging or corrosion) to the machine in which they are being employed (Pronobis, Virmond, El-Nashaar). This leads to a major disadvantage of biofuels, the lack of worldwide standards for their elemental composition (Saidur). By enforcing limits on the abundance of specific elements biofuels contain, equipment, money, and time may all be saved. This has led to research on the composition of various biomass.

Analysis of both the major and minor elemental species present in various biofuels, biomass, and their respective ash products have been conducted (El-Nashaar, Voli, Cuiping, Woods, Baernthaler). Silicon is one of the species that is typically considered. Concentrations (mg of Si/kg of biomass) have resulted in values of 541 mg/kg of a wood and bark biomass (Baernthaler), 19,400 mg/kg of straw biomass (Baernthaler), 5,500 to 32,400 mg/kg of perennial grasses (Voli), and 1,847 to 28,620 mg/kg of various temperate grasses (El-Nashaar). While the amount of silicon present is important, the particle growth and morphology during combustion is likely to provide a clearer picture of how particulates may interfere with industrial processes.

Various studies have been performed on silica aggregates in different combustion environments and during different stages of the combustion process. These studies consider environments such as premixed flames, diffusion flames, aerosol reactors, and furnaces. These studies employ different techniques such as emission, nuclear magnetic resonance (NMR), mass spectrometry (MS), small- or ultra-small-angle x-ray scattering (SAXS/USAXS), 90° light scattering (90° LS), transmission electron microscopy (TEM), scanning electron microscopy (SEM), dynamic light scattering (DLS), and angle-dependent light scattering (ADLS)[1]. Silicon is usually introduced into these environments either through the chemical tetraethyl orthosilicate (TEOS), $C_8H_{20}O_4Si$, silane, SiH_4, silicon tetrachloride, $SiCl_4$, or hexamethyldisiloxane (HMDSO), $C_6H_{18}Si_2O$. A collection of publications illustrating the diversity in these studies can be seen in Table 1.

[1] Angle-dependent light scattering has also been termed in the literature as light scattering dissymmetry (Zachariah), multiangular laser light scattering (Kim), static light scattering (Hurd), or simply light scattering (G. Wang, Sorensen 2001). For clarity, this paper will employ the term angle-dependent light scattering (ALDS) (Souza).

Reference	Combustion Environment	Technique(s)	Si Seeder
Flower	CH_4/O_2 Premixed Flame	DLS, TEM	HMDSO
Hurd	CH_4/Air Premixed Flame	DLS, ADLS, TEM	HMDSO
Zachariah	H_2/O_2 Counterflow Diffusion Flame Reactor	DLS, ADLS	SiH_4
Chagger	CH_4/N_2/Air Diffusion Flame	Emission Spectroscopy	HMDSO
Choi	H_2/O_2/He/N_2 Diffusion Flame	90° LS, TEM	$SiCl_4$
Cho	H_2/O_2/He/N_2 Diffusion Flame	90° LS, TEM	$SiCl_4$
G. Wang	900° C Furnace	ADLS	TEOS
Cutler	$H_2/O_2/N_2$ Premixed/Diffusion Flames	NMR, MS, TEM	HMDSO
Kim	CH_4/Air Premixed Flame	ADLS, TEM	$SiCl_4$
Han	CH_4/Air/N_2 Premixed Flat Flame Aerosol Reactor	SEM	$SiCl_4$
Kammler	$CH_4/O_2/N_2$ Aerosol Reactor	USAXS, TEM	HMDSO
Camenzind	CH_4/O_2 Diffusion Flame	SAXS, TEM	HMDSO
Smirnov	CH_4/Air Premixed Flame	TEM	HMDSO

Table 1: A collection of publications illustrating the diversity of silica aggregate studies in combustion environments.

While these studies provide insight for the growth and aggregation of silica particles in a combustion environment, few study a range of variables such a silicon seeding concentrations, flame temperatures, and equivalence ratios throughout an entire flame. The goal of this study is to employ ADLS in order to determine the effects of silicon seeding concentrations and flame temperature on a lean, stoichiometric, and rich methane/air premixed flame seeded with HMDSO.

2. Methods

Premixed methane/HMDSO/air flat flames were produced on a porous plug burner with a diameter of 6 cm. The burner has been used in previous studies and is well characterized (Smirnov, Mokhov). The measurements were carried out in a 1950 K stoichiometric flame environment. Flame temperature was determined using the same procedure found in (Smirnov) and compared to measurements in (Mokhov) The flow rates of methane and air were measured with Bronkhorst flow meters having an accuracy of 3%. Before mixing, a fraction of the methane gas was bubbled through HMDSO (Sigma-Aldrich/Fluka 52630, ≥98.5% pure). The concentration of HMDSO that is introduced into the fuel mixture is dependent on the overall pressure of the gas flow and is varied by changing the flow rate of gas that passes through the bubbler. HMDSO concentration (χ_{HMDSO}) is calculated using the following equation:

$$\chi_{HMDSO} = \frac{\frac{P_{HMDSO}}{P_{Bub}} \times Q_{Bub}}{Q_{Total} + \frac{P_{HMDSO}}{P_{Bub}} \times Q_{Bub}} \quad (1)$$

where P_{HMDSO} is the vapor pressure of HMDSO, 5.59 kPa at 298 K (Flaningam), P_{Bub} is the pressure in the bubbler, Q_{Bub} is the flow rate of methane through the bubbler, and Q_{Total} is the total measured flow rate, or the sum of the measured flow rates of air, methane, and methane through the bubbler. This relationship has been confirmed by measurements in (Smirnov).

The excitation source was a 532 nm laser (Klastech Laser Tech) with a power of approximately 1 W. The light was first chopped at a frequency of 650 Hz, traveled through a lens, which focused the beam at the center of the burner, through an iris, through the flame, and eventually into a beam dump. The laser, chopper, lens, and iris were contained in a housing in order to prevent the detection of stray reflections and for safety. The burner was positioned on a vertical translation stage (10 cm, Parker) to vary the height above the burner (HAB) at which measurements were performed. The scattered light was collected at various angles through a lens tube system (Hamamatsu) attached to a photomultiplier tube, PMT (Hamamatsu H10721-210). The lens tube system housed a filter and lens (100 mm focal length). The PMT had a collection area with an outer diameter 8 mm. The PMT was positioned so that it was 40 cm from the center of the burner at all collection angles providing the sample area in the flame of 8 mm. The PMT signal was measured by a lock-in amplifier (EG & G Instruments 7265 DSP).

The PMT and collecting lens were placed on a system containing two translation stages, long (1m, Standa 8MT295-1040-10) and short (30 cm, ThorLabs LTS200/M), and a rotation stage (Standa 008729). The long axis was positioned so that it was the hypotenuse of a right triangle with the other two sides being 40 cm long and meeting at the center of the burner (Figure 2). The short axis is perpendicularly mounted on top of the long axis. These two axes work in tandem to keep the PMT at 40 cm from the burner center at all angles. On top of the short axis was the rotational stage. This was used to keep the PMT directed at the center of the flame. The PMT setup was arranged so that the center of the PMT was the same height as the laser beam.

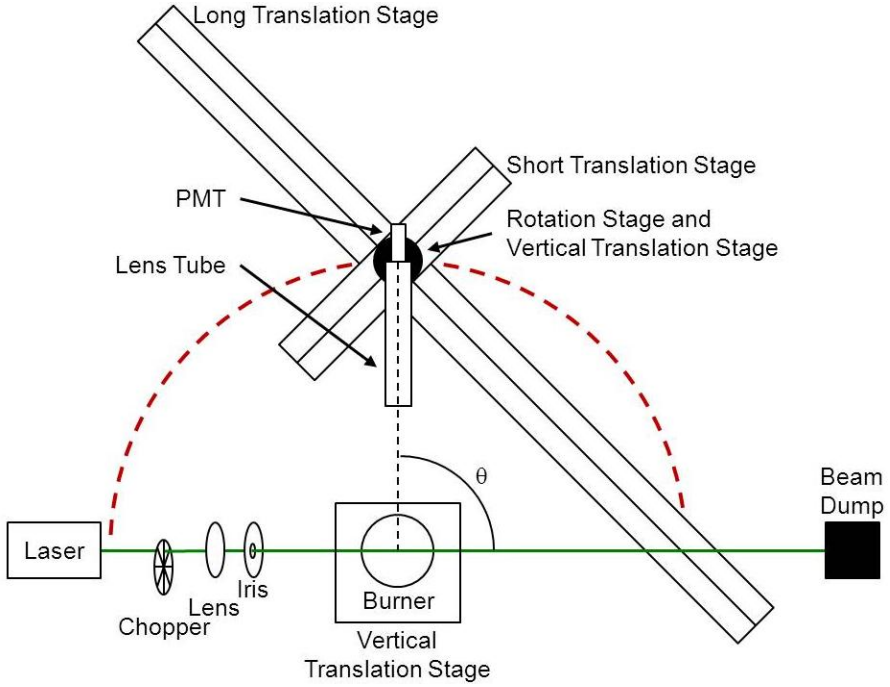

Figure 2. Experimental setup for angle-dependent light scattering. The red dashed line represents the arc on which various detection angles (θ) are located. Excitation laser (green line) is λ = 532 nm. 90° detection shown.

First, the PMT was aligned to maximize the signal at a 90° collection angle. Once this was determined, the location of the short axis on the long axis, the location of the rotation stage on short axis, and the amount of rotation needed for each detection angle were calculated. This was done for detection angles (θ) of approximately 40° to 120° in 10° increments. Data was collected for a 1950 K stoichiometric (φ = 1.0) flame with varying concentrations of HMDSO (200, 300, 400 ppm). In each flame data was collected at a HAB of 10 – 60 mm in increments of 10 mm.

3. Results and Discussion

Theory and treatment of ADLS data has been well described. A brief description will be provided here, but for more information the authors recommend Sorensen 2001 and Souza.

Fractal aggregates can be observed in many various natural settings, e.g. snowflakes, and are commonly found in flame particulate, e.g. soot. Some oxides are also known to produce fractal aggregates in a flame environment, including titania, TiO_2, and silica, SiO_2. Fractal aggregates are characterized by the number of primary particles in the aggregate (N), the size, specifically the radius, of the primary particles (a), the radius of gyration (R_g), and the fractal dimension (D_f). The relationship between these variables is:

$$N = k_0 \left(\frac{R_g}{a} \right)^{D_f} \tag{2}$$

where k_0 is a proportionality constant. The values of these variables can be determined via TEM analysis, however, it is a very time consuming and tedious process (Sorensen 2001). The radius of gyration can be found using only 90˚ light scattering, however, one must know the values of a and D_f, typically determined using TEM. This proves difficult when desiring a flame profile as a may be dependent on the height of the measurement (Smirnov). ADLS and Guinier analysis provide a quicker, nonintrusive, and often times cheaper approach to characterizing fractal aggregates in a flame. Because ADLS measurements can be taken much faster, a larger area of the flame and various conditions can be studied (Sorensen 2001, Souza).

In order for ADLS and Guinier analysis to be applicable the size of the aggregates (R_g) must be smaller than q^{-1} where q is the so-called scattering vector determined by the following expression:

$$q = \frac{4\pi}{\lambda}\sin\left(\frac{\theta}{2}\right) \quad (3)$$

λ is the incident laser wavelength and θ is the angle of detection (see Figure 2). Figure 3 provides a typical example of dependence of the intensity $I(q)$ upon the scattering vector q. Figure 3 is an adaptation of Figure 22 in (Sorensen 2001). Also visible in Figure 3 is what is known as the Power Law Regime. If this is observed, then one can determine the fractal dimension, D_f, by determining the slope of the linear region.

In the Guinier Regime, R_g can be determined using the relationship (Sorensen 2001):

$$\frac{I(0)}{I(q)} \simeq 1 + \frac{1}{3}R_g{}^2 q^2 \quad (4).$$

By plotting $1/I(q)$ as a function of q^2 and fitting the data linearly one can determine that I(0) is the inverse of the y-intercept and thus R_g can be determined using the value of the slope of the line. An example of a Guinier Analysis plot can be seen in Figure 4.

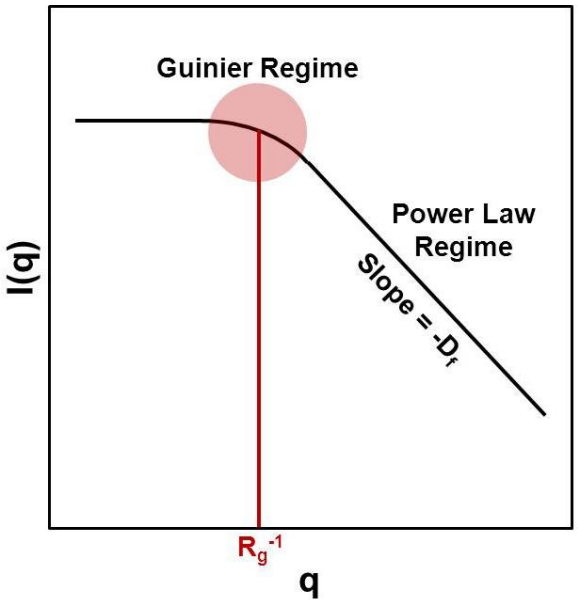

Figure 3. A plot illustrating the relationship between signal and detection angle, specifically pointing out the Guinier regime, where $R_g < q^{-1}$. This plot is an adaptation from Sorensen 2001.

In the present work, R_g has been determined for various heights of three flames with various HMDSO concentrations. These values are presented in Table 2 and plotted in Figure 5. The data for HMDSO concentrations of 200 and 300 ppm do not show a linear growth pattern as 400 ppm does. While the data are noisy for 200 ppm and 300 ppm, the growth pattern and the average size of the aggregates determined for the 200 ppm flame are similar to data collected in a similar flame using TEM (Smirnov).

HAB (mm)	200 ppm	300 ppm	400 ppm
60	59.97	52.58	141.71
50	73.86	62.36	121.31
40	58.93	53.30	103.12
30	62.66	47.72	95.20
20	58.25	16.74	75.79

Table 2: R_g (nm) at various HAB (mm) for 1950 K stoichiometric flames with varying concentrations of HMDSO.

Returning to the condition of $R_g < q^{-1}$, in the present experiments q was varied from 9.98 to 17.76 μm^{-1}. R_g values varied from 0.017 to 0.142 μm. Therefore, depending on the angle this condition is not always met. However, Sorensen has addressed this issue and has shown that it is acceptable to use data outside this regime for fractal aggregate analysis. It is possible to relax the condition to $R_g \leq 2q^{-1}$ or even $R_g \leq 3q^{-1}$ (Sorensen 2001). Data presented here falls well within this regime

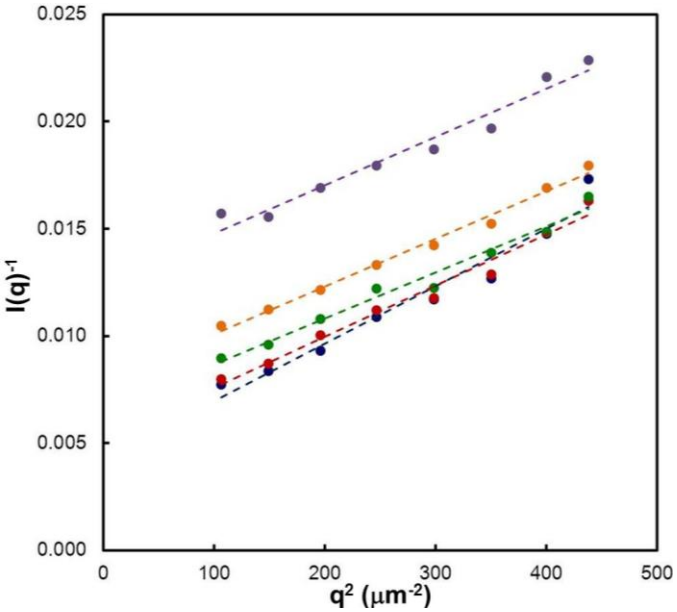

Figure 4. Guinier analysis for a 1950 K stoichiometric flame with χ_{HMDSO} = 400 ppm for heights above the burner of 20 mm (purple), 30 mm (orange), 40 mm (green), 50 mm (red), and 60 mm (blue).

4. Conclusions

This research has provided a method and starting point for a better understanding of the growth of SiO_2 aggregates in a 1950 K stoichiometric flame. Future studies will include perfecting data collection parameters and alignment along with studying the effects of temperature, equivalence ratio, and a greater range of HMDSO concentrations. These results along with similar studies planned to be conducted in the near future hope to provide beneficial results to those looking to employ silicon containing biofuels in various industrial applications.

Acknowledgements

This research was funded by a grant of the Energy Delta Gas Research (EDGaR) program. We also gratefully acknowledge partial support of the Russian Foundation for Basic Research (project No. 12-02-00123-a).

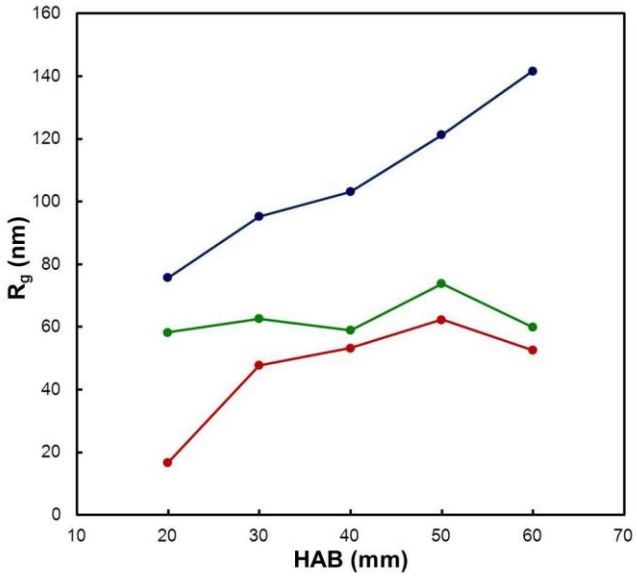

Figure 5. R_g as a function of height above the burner for HMDSO concentrations of 400 ppm (blue), 300 ppm (red), and 200 ppm (green).

References

Baernthaler, G., Zischka, M., Haraldsson C., Obernberger, I. Biomass and Bioenergy, 30 (2006) 983 - 997.

Camenzind, A., Schulz, H., Teleki, A., Beaucage, G., Narayanan, T., Pratsinis, S.E. European Journal of Inorganic Chemistry, 2008 (2008) 911 - 918.

Chagger, H.K., Hainsworth, D., Patterson, P.M., Pourkashanian, M., Williams, A. Symposium (International) on Combustion, 26 (1996) 1859 - 1865.

Cho, J., Choi, M. Journal of Aerosol Science, 31 (2000) 1077 - 1095.

Choi, M., Cho, J., Lee, J., Kim, H.W. Journal of Nanoparticle Research, 1 (1999) 169 - 183

Cuiping L., Chuangzhi W., Yanyongjie, Haitao H., Biomass and Bioenergy, 27 (2004) 119 - 130.

Cutler, C.J., Hayhurst, A.N., Wynn, E.J.W. Proceedings of the Combustion Institute, 29 (2002) 1047 - 1054.

El-Nashaar, H.M., Griffith, S.M., Steiner, J.J., Banowetz, G.M. Bioresource Technology, 100 (2009) 3526 - 3531.

Flaningam, O.L. Journal of Chemical and Engineering Data, 31 (1986) 266 – 272.

Flower, W.L., Hurd, A.J. Applied Optics, 26 (1987) 2236 – 2239.

Han, J., Chang, H., Lee, J., Chang, H. Aerosol Science and Technology, 37 (2003) 550 - 564.

Hurd, A.J., Flower, W.L. Journal of Colloid and Interface Science, 122 (1988) 178 - 192.

Internal Energy Agency, in, Organisation for Economic Co-operation and Development, Paris, 2012.

Kammler, H.K., Beaucage, G., Kohls, D.J., Agashe, N., Ilavsky, J. Journal of Applied Physics, 97 (2005) 054309-054301 - 054309-054311.

Kim, H.W., Choi, M. Journal of Aerosol Science, 34 (2003) 1633 - 1645.

Ministry of Economic Affairs, Agriculture and Innovation. Energy Report 2011. The Hague, 2011.

Mokhov, A.V., Levinsky, H.B. Proceedings of the Combustion Institute, 28 (2000) 2467 – 2474.

Office of Survey Deveolpment and Statistical Integration, U.S. Energy Information Administration, U.S. Department of Energy. Annual Energy Review 2011. Washington, D.C. 2011.

Pronobis, M. Biomass and Bioenergy, 28 (2005) 375 - 383.

Saidur, R., Abdelaziz, E.A., Demirbas, A., Hossain, M.S., Mekhilef, S. Renewable and Sustainable Energy Reviews, 15 (2011) 2262 - 2289.

Smirnov, B.M., Dutka M., van Essen, V.M., Gersen, S., Visser, P., Vainchtein, D., De Hosson, J.T.M., Levinsky, H.B., Mokhov, A.V. A Letters Journal Exploring the Frontiers of Physics, 98 (2012) 66005.

Sorensen, C.M., Cai, J., Lu, N. Applied Optics, 31 (1992) 6547 – 6557.

Sorensen, C.M. Aerosol Science and Technology, 35 (2001) 648 - 687.

Souza, G.R., Miller, J.H. Elastic Light Scattering of Biopolymer/Gold Nanoparticles Fractal Aggregates, in: C.D. Geddes (Ed.) Reviews in Plasmonics 2010, Springer, 2012, pp. 39 – 68.

Vamvuka, D., Zografos, D. Fuel, 83 (2004) 2051 - 2057.

Vassilev, S.V., Baxter, D., Andersen, L.K., Vassileva, C.G. Fuel, 105 (2013) 40 - 76.

Virmond, E., Sena, R.F., Albrecht, W., Althoff, C.A., Moreira, R.F.P.M., Jose, H.J. Waste Management, 32 (2012) 1952 - 1961.

Voli, K.P., David, M.B., Tsai, J., Voigt, T.B., Darmody, R.G., Mitchell, C.A. Biomass and Bioenergy, 35 (2011) 2807 - 2813.

Wang, G., Sorensen, C.M. Applied Optics, 41 (2001) 4645 - 4651.

Wang, W., Zheng, Y., Liu, X., Wang, P. Energy and Fuels, 26 (2012) 6047 - 6052.

Woods, G.D., Fryer, F.I. Analytical and Bioanalytical Chemistry, 389 (2007) 753 - 761.

Zachariah, M.R., Chin, D., Semerjian, H.G., Katz, J.L. Applied Optics, 28 (1989) 530 - 536.